THE ASTROPHYSICAL JOURNAL, 472:349–359, 1996 November 20

THE ENVIRONMENT OF V633 CASSIOPEIAE AND V376 CASSIOPEIAE: EVIDENCE FOR CIRCUMSTELLAR DISKS

LOUIS ASSELIN,[1] FRANÇOIS MÉNARD,[2,3] PIERRE BASTIEN,[1,3] JEAN-LOUIS MONIN,[2,3] AND DANIEL ROUAN[3,4]
Received 1991 August 13; accepted 1996 June 4

ABSTRACT

We present optical direct and polarimetric imaging, optical polarimetry, and infrared direct imaging of the Herbig Ae/Be stars V633 Cas (=LkHα 198) and V376 Cas. Both stars are associated with extended reflection nebulosities.

V633 Cas appears as a single object associated with an extended optical nebula oriented northwest-southeast with a mean position angle of 128°. This nebula, having the form of a large "loop," traces the redshifted lobe of a CO outflow. Various features are present within the circumstellar medium of V633 Cas. The position of the star does not change with wavelength within the uncertainties. We suspect its linear polarization to be time variable. The polarization pattern close to V633 Cas suggests that another source, possibly the infrared source 6″ north of V633 Cas, V633 Cas B, is the most probable candidate to drive the large-scale outflow.

For V376 Cas, high-resolution images with very good seeing in *R* and [S II] filters show for the first time two peaks in the isophote contours, about 1″ apart. Also, V376 Cas has the largest linear polarization observed so far in a young stellar object, ≈23% at a position angle of ≈26°. This is well explained if an edge-on circumstellar disk is present. Polarization maps of V376 Cas showing a pattern of aligned vectors and two null points support this explanation. Further support comes from the detection of two intensity peaks that can be explained by the presence of a reflection nebula whose center is hidden by an optically thick disk seen edge-on. A less preferable explanation would be the presence of enhanced line emission regions due to shocks in recollimating flows. We exclude the possibility that V376 Cas is a binary star with a 1″ separation.

Subject headings: binaries: visual — polarization — stars: individual: (V633 Cassiopeiae, V376 Cassiopeiae) — stars: pre–main-sequence

1. INTRODUCTION

Herbig Ae/Be stars are intermediate-mass pre–main-sequence stars. It has been known for a long time that these stars are often associated with optical reflection nebulosities (Herbig 1960). Because of the numerous spectroscopic and photometric properties they share with the low-mass pre–main-sequence T Tauri stars, it is tempting to suppose that their circumstellar environments are also similar. However, even if the models with accretion disks may explain many of their observed properties (Hillenbrand et al. 1992; Lada & Adams 1992), the evidence for the very presence of these disks around Herbig Ae/Be stars is not as convincing as for the T Tauri stars, and other interpretations in which the star has a more dominant role have been proposed (e.g., Catala 1989; Böhm 1993). Böhm (1993) argues that the absence of veiling on optical photospheric lines and the shape of forbidden lines rule out the presence of an accretion disk and proposes an alternative model involving a strong chromosphere and a stellar wind.

Longward of 50 μm, recent observations of Herbig Ae/Be stars with large infrared excess, including V633 Cas, suggest that it is dust located in a large circumstellar envelope rather than an accretion disk that is responsible for the emission (Natta et al. 1992, 1993). However, these authors argue also that these envelopes have to be heated by sources much cooler than indicated by the spectral type of the central stars, accretion disks being good candidates for the heat sources. They measure typical envelope sizes of 10^4 AU. Similar extension for circumstellar structures are seen in millimeter and submillimeter observations, and on polarization maps of many of these objects (e.g., R Mon, PV Cep, R CrA; Ménard 1993).

The exact nature of the circumstellar environment of Herbig Ae/Be stars is therefore quite complicated, and to a great extent, uncertain. With the goal to obtain a better picture of this environment, we decided to focus our attention on two stars located in Cassiopeia, V376 Cas and V633 Cas (better known as LkHα 198). These stars are good candidates because they show extended optical reflection nebulae (Bastien et al. 1989), and one of them, V376 Cas, is the most highly polarized young stellar object (YSO) known to date. Because the polarization is produced by scattering on dust grains, it is linked tightly to the distribution of material around a star, and we can hope that polarization maps, together with aperture polarimetry, will complement direct imaging and give us additional information about the structure of the various components of the circumstellar material.

Recently, other sources have been found in the vicinity of these two stars. Lagage et al. (1993) found, at 10 μm, a source located 6″ north of V633 Cas. This star, V633 Cas B, was also seen by Corcoran, Ray, & Bastien (1995, hereafter CRB) in the *K* band. Another source was detected at 1.1

[1] Observatoire du Mont Mégantic and Département de Physique, Université de Montréal, B.P. 6128, Succ. Centre-ville, Montréal, Québec H3C 3J7, Canada.
[2] Laboratoire d'Astrophysique, Observatoire de Grenoble, B.P. 53X, F-38041 Grenoble CEDEX, France.
[3] Guest observer at the Canada-France-Hawaii Telescope.
[4] DESPA, Observatoire de Paris, 5 Place Jules-Janssen, F-92195 Meudon Cedex, France.

mm ≈ 21″ NW of V633 Cas by Hajjar & Bastien (1994, 1996).

In the next section (§ 2) we present the observations. The immediate results are presented in § 3. In § 4, we discuss the morphology of the circumstellar environment we can deduce for both stars as well as implications for the binary formation scenarios. A short enumeration of the main results summarizes the paper in § 5.

2. OBSERVATIONS

The polarization measurements were obtained on the 1.6 m Ritchey-Chrétien telescope of the Observatoire du Mont Mégantic (OMM) in Québec during the period 1986 August 5–14. The polarimeter is similar to the one described by Angel & Landstreet (1970). Two filters centered at 7675 Å and 4700 Å (bandwidths are 2450 Å and 1800 Å, respectively) were used together with an 8″.3 diaphragm. Instrumental and sky polarizations were evaluated carefully and subtracted from the measurements.

Polaro-images were obtained at OMM by inserting and rotating a Polaroid HN38 polarizer in the incident beam in front of the filters on 1986 August 26 and 1989 September 28. We select the *V* and *I* filters for polaro-imaging because they transmit virtually no emission lines from YSOs. They are well suited to study the scattered light component. On the other hand, the *R* wave band contains many emission features, e.g., [O I] λλ6300, 6363, [N II] λλ6548, 6584, Hα, and [S II] λλ6717, 6731 as well as a scattered component superimposed on the stellar continuum. This filter should not be used for polarimetric imaging purposes because the presence of these emission lines renders the interpretation of the maps very difficult, at best.

Direct images were obtained at OMM and at the Canada-France-Hawaii telescope (CFHT). At OMM, an RCA chip (512 × 320 with pixel size of 30 μm giving 0″.48 per pixel) was used to obtain *UBVRI* images on 1989 September 25–27. At CFHT, on 1989 December 3–5, both stars were imaged through narrow-band filters centered on the [S II] and Hα emission lines and through a standard *R* filter. The RCA2 CCD, 640 × 1024 pixels (0″.11 per pixel), was used. Another image was taken on 1993 December 12 with the high-resolution camera (HR Cam) in Hα. The [S II] filter we used transmits both lines at λλ6717, 6731, and the Hα filter also includes [N II] λ6584.

The appropriate data reduction procedures were performed. Dome and sky flat fields were collected in both the direct and polarimetric imaging modes. Bias, dark current, and sky contributions were subtracted from the frames. Also, to allow deconvolution of the 1989 CFHT image set by a maximum entropy method, the stars SAO 21265 and GL 905.2 B were used to determine the point-spread function (PSF).

The CIRCUS camera (Rouan, Lacombe, & Tiphène 1990) attached to the CFHT was also used to obtain a *K*-band (2.2 μm) image of V376 Cas on 1991 December 16. CIRCUS is equipped with a 128 × 128 InSb detector optimized for observations at 2 μm and longward. The detector has a very large integration capacity (≈40 × 10^6 electrons) so that long integration times are possible and the images are background noise limited from 2.2 to 4.8 μm. The focal plate scale was measured on the HL/XZ Tau system to be 0″.28 per pixel, well adapted to the CFHT sub-arcsecond seeing conditions (≈0″.6 during the observations). The star BS 9045 was used as a PSF reference; every frame on the source was followed by one on the nearby sky (40″ chopping throw in R.A.). The sky background was subtracted, the images were flat-fielded, and the bad pixels were removed.

Table 1 gives the log of the observations. The columns give (1) the filter, (2) the exposure time, (3) the position angle of the polarizer for the polarized images, (4) the air mass at midexposure time, (5) the mean FWHM of the stellar profiles (measured on the median frame when more than one frame is available), (6) the date of observation, (7) the number of frames obtained, and (8) the telescope used.

TABLE 1

LOG OF THE OBSERVATIONS

Filter (1)	Exposure Time (s) (2)	Θ_{pol} (deg) (3)	Air Mass (4)	FWHM (arcsec) (5)	Date (6)	*N* (7)	Telescope[a] (8)
V	600	0	1.097	2.75	1986 Aug 26	2	M
	600	60	1.052	2.47	1986 Aug 26	2	M
	600	120	1.074	2.37	1986 Aug 26	2	M
I	240	...	1.232	2.41	1989 Sep 25	1	M
	180	...	1.205	2.37	1989 Sep 25	4	M
R	480	...	1.113	2.53	1989 Sep 25	4	M
V	1800	...	1.063	2.77	1989 Sep 25	1	M
	3600	...	1.039	2.97	1989 Sep 25	1	M
B	3600	...	1.031	2.85	1989 Sep 27	2	M
U	1061	...	1.031	2.03	1989 Sep 27	1	M
	800	...	1.108	2.00	1989 Sep 27	1	M
	1800	...	1.141	2.05	1989 Sep 27	1	M
I	400	0	1.028	2.25	1989 Sep 28	6	M
	400	30	1.029	2.25	1989 Sep 28	6	M
	400	150	1.031	2.25	1989 Sep 28	6	M
R	100	...	1.300	0.86	1989 Dec 4	1	C
[S II].....	1800	...	1.292	0.73	1989 Dec 4	2	C
R	200	...	1.289	0.85	1989 Dec 5	1	C
	150	...	1.287	0.83	1989 Dec 5	1	C
Hα	1200	...	1.289	1.31	1989 Dec 5	2	C
K	8	...	1.408	0.6	1991 Dec 16	50	C
Hα	900	...	1.369	0.8	1993 Dec 12	1	C

[a] C = CFHT; M = Mont Mégantic.

3. RESULTS

3.1. *Polarimetry*

The linear polarization measurements are presented in Table 2. The columns give respectively the name of the object, the Julian Date corresponding to the middle of each observation, the linear polarization P in percent, its associated error from photon counting statistics σ_P in percent, the equatorial position angle θ in degrees measured eastward of north, its error σ_θ in degrees, and the filter used. The errors on the position angles are at least 1°, to take into account possible calibration errors.

A variability analysis can be performed on the polarization data following the method described by Bastien (1982), which compares the observed scatter in the data with the observational errors and computes a χ^2 and the possibility of finding this χ^2 for both the Q and U parameters separately. The $P(\chi^2)$ values, computed with 1.5 times the observed Poissonian errors, are given in Table 3. The measures given by Leinert, Haas, & Lenzen (1991, hereafter LHL) cannot be used for this analysis because they give only the polarization after correction for interstellar polarization and not the observed data. Also, they averaged their measurements obtained with two different diaphragm sizes.

The two measurements of V633 Cas at 7675 Å give no indication of variability. However, taking into account the polarization values calculated from the CCD images, V633 Cas should be considered as "suspected variable." On the other hand, although V376 Cas does not seem to vary at 4700 Å, the four measurements at 7675 Å indicate very clearly that its polarization is variable in the red.

TABLE 2

LINEAR POLARIZATION DATA

Object	JD (+2,446,600)	P (%)	σ_P (%)	θ (deg)	σ_θ (deg)	Filters[a]
V376 Cas.....	47.699	23.74	0.49	30.2	1.0	1
	48.774	23.73	0.26	26.2	1.0	1
	55.609	21.97	0.30	26.2	1.0	1
	55.769	19.53	0.28	25.0	1.0	2
	56.670	19.29	0.28	25.4	1.0	2
	56.710	21.57	0.23	24.6	1.0	1
*V*633 Cas.....	47.676	2.14	0.29	32.4	3.9	1
	48.723	1.65	0.23	18.7	3.9	1

[a] (1) = Schott RG-645 (λ_c = 7675 Å, FWHM = 2450 Å); (2) = Corning 4-96 (λ_c = 4700 Å, FWHM = 1800 Å).

TABLE 3

POLARIZATION VARIABILITY ANALYSIS

Star	λ(Å	N[a]	$P(\chi^2_Q)$	$P(\chi^2_U)$	Variability
V376 Cas.....	4700	2	0.458	0.016	?
	7675	4	0.994	1.000	yes
V633 Cas.....	7675	2	0.528	0.908	Suspected

[a] Number of individual measurements.

3.1.1. *V376 Cas*

With ≈23% in the red, V376 Cas is the YSO with the largest integrated linear polarization measured so far. The polarization is lower in the blue but still very large, ≈19%. LHL measured 7.2% ± 0.2% and 30° ± 2° at 1.65 μm (H band). A large circular polarization (0.5%) has been detected by Gravel & Bastien (1996). The polarization is larger at longer wavelengths in the optical, as can be seen from Tables 2 and 4 and also from LHL's optical measurements.

This large a polarization clearly cannot be due to aligned interstellar grains (LHL). A scattering origin is probable, given that there is a significant amount of extinction in front of the source to absorb the direct unpolarized starlight, which in turn implies multiple scattering. The high circular polarization that has been detected also argues for multiple scattering (Gravel & Bastien 1996).

3.1.2. *V633 Cas*

From Table 2, V633 Cas has a modest linear polarization, of order ~2%. This is surprising in view of the large amount of circumstellar material surrounding it (see Fig. 1) because a large contribution from scattered (hence polarized) light is expected in that case. However, the linear polarization is nearly perpendicular to the large-scale bubble that delineates the outflow direction (e.g., Nakano et al. 1990). At first sight, it seems that this is another case in which the jet (or outflow) associated with a YSO is aligned perpendicularly to the direction of the integrated linear polarization. This would favor models involving dust grains in the jets and/or multiple scattering in a circumstellar disk (Bastien 1987; Bastien & Ménard 1988, 1990). However, the

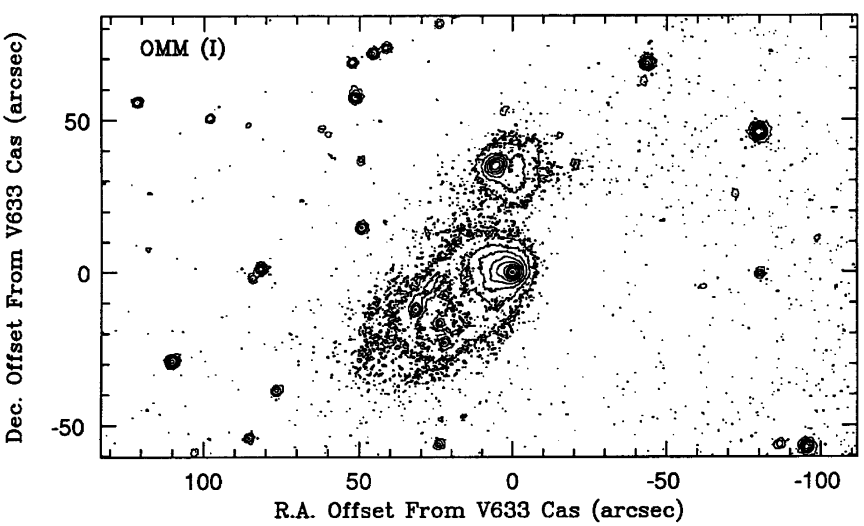

FIG. 1.—I-image of the field toward V633 Cas and V376 Cas. The image is from OMM. Contours are scaled logarithmically from the peak down to 2.5 σ above local sky level. V376 Cas is located ≈37″ north of V633 Cas. Offset positions are measured from V633 Cas. North is up, and east is to the left.

jet, HH 162, found to be associated with V633 Cas by CRB, is at a position angle of 160°, not perpendicular to the linear polarization vector as expected. This might be caused by contamination of the polarization by the nearby infrared source V633 Cas B, since the diaphragm used has a diameter (8″.3) comparable to the separation between the two stars, and also because the polarization map close to the star is quite complex (see below).

3.2. *Polarization Maps*

Optical linear polarization maps of V376 Cas and V633 Cas are presented in Figures 2 and 3, respectively. The linear polarization is traced by a grid of vectors showing the magnitude and orientation of the electric field at different locations in the nebula. Binning to $\approx 1''$ is done to improve the signal-to-noise ratio and the clarity of the plot. This value is also well adapted for a good sampling of the seeing. We point out that the V and I polarization maps were taken more than 3 years apart, so that variability may also contribute, in addition to the different passbands, to differences between the two maps.

The integrated polarization values, centered on the sources, are given in Table 4 for both objects. The results are compatible with the aperture polarization measurements presented in § 3.1. It should be noted that the data reduction procedure, based on the assumption that the field stars have a zero polarization for scaling, corrects for the effects of interstellar polarization. Although not perfect, this

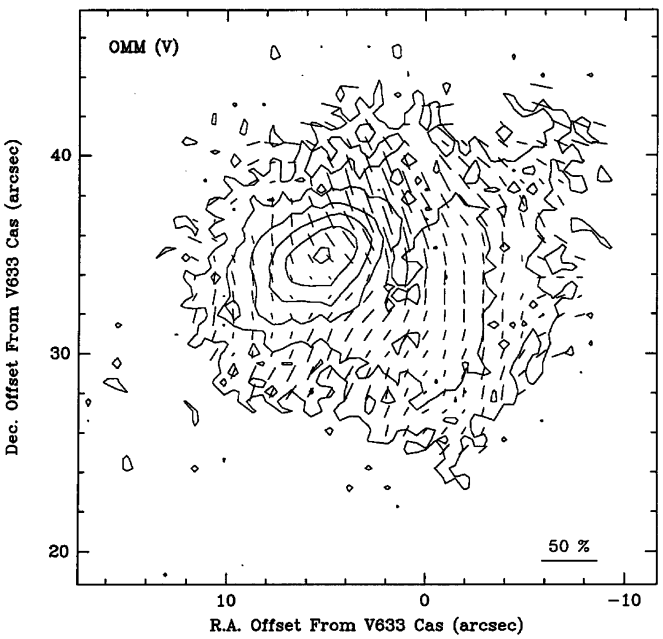

FIG. 2*a*

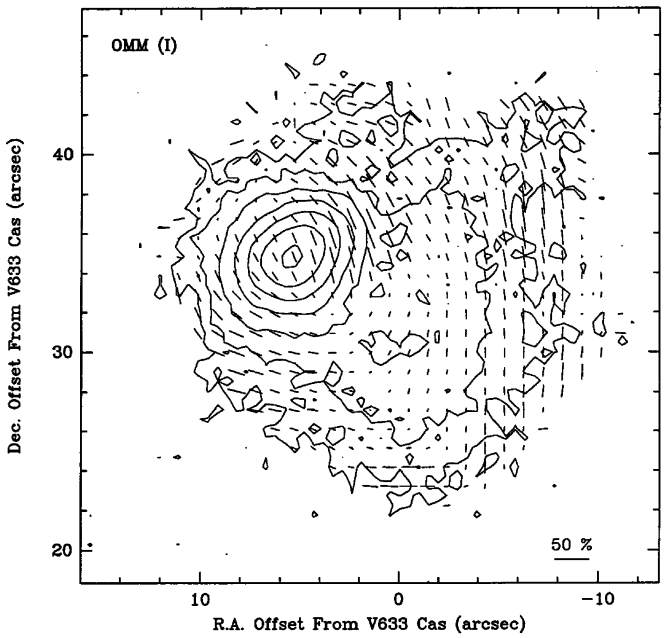

FIG. 2*b*

FIG. 2.—Optical linear polarization map of V376 Cas obtained at the OMM at (*a*) 5450 Å and (*b*) 8100 Å. The length of the polarization vector (*E*-field) is proportional to the degree of polarization; the scale is given in the lower right corner. For clarity, the polarization is plotted every second pixel. The intensity contours are scaled logarithmically down from (*a*) peak to 2 σ and (*b*) peak to 1 σ.

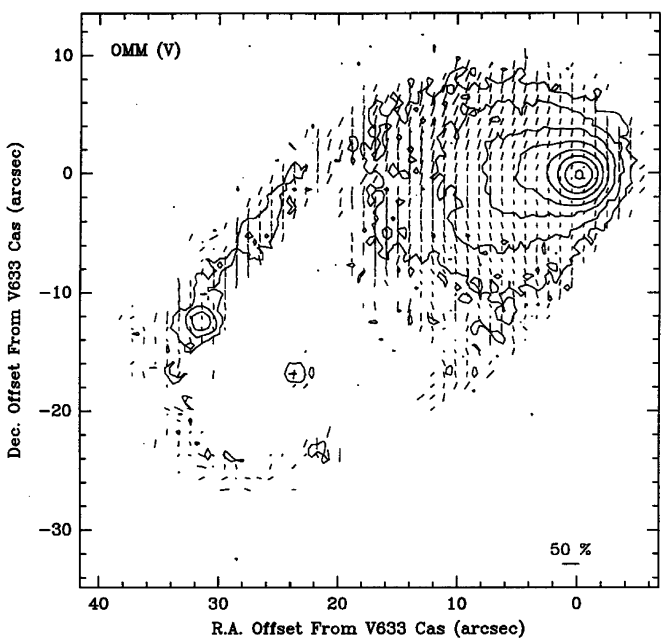

FIG. 3*a*

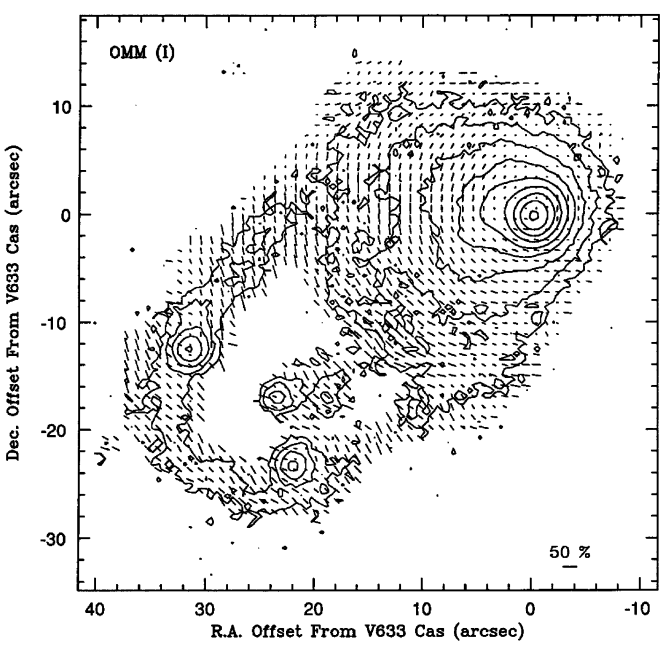

FIG. 3*b*

FIG. 3.—Same as Fig. 2, but for V633 Cas

TABLE 4

LINEAR POLARIZATION DATA FROM THE POLARIZATION MAPS

Object	P (%)	σ_P (%)	θ (deg)	σ_θ (deg)	λ (Å)	Box Size[a] (arcsec)
V376 Cas.....	22.6	1.1	24.2	1.4	5450	4
	15.9	0.5[b]	23.4	0.6	5450	8
	27.2	0.4	27.5	0.4	8100	4
	14.6	0.5[b]	27.4	1.0	8100	8
V633 Cas.....	2.4	0.5	26.9	6.6	5450	3
	5.0	0.5[b]	25.7	2.9	5450	8
	6.1	0.4	173.7	1.9	8100	8
	3.0	0.5[b]	112.9	4.8	8100	8

[a] Size of the binning box centered on the star.

[b] The formal statistical errors are very small. However, calibration errors such as flat-field correction limit the true errors.

technique is a good first step to remove the interstellar polarization, since many stars are used to calculate the scaling factor between two images made with the analyzer at different orientations.

The polarization levels in the reflection nebula are also informative. For V376 Cas we do not observe values (as high as 50%) observed in the northwestern lobe by LHL at 9000 Å. Our values are $\simeq$15% at 5450 Å and $\simeq$25% at 8100 Å. For V633 Cas, on the other hand, the polarization goes up to 50% in V and up to 68% in I. For both objects, such large values indicate that the nebulosities are seen mainly in reflection, with the polarization arising from single scattering of starlight, most probably by dust grains.

3.2.1. *V376 Cas*

For V376 Cas (Fig. 2), the general pattern of the polarization is centrosymmetric except close to the source, where aligned vectors are observed. Two polarization null points are present at the tips of the aligned vector zone. They mark the position at which the polarization goes to zero between the aligned vectors and the centrosymmetric pattern (Scarrott, Draper, & Warren-Smith 1989; Bastien & Ménard 1990). Their positions are given in Table 5, where the R-coordinate is defined parallel to the direction of the integrated polarization of the star ($\approx$26° for V376 Cas) and Z is perpendicular to it. We notice that V376 Cas is not colinear with the null points. This aligned vector pattern has also been observed by Piirola, Scaltriti, & Coyne (1992) in the I band and by LHL at 9000 Å. We notice that the area with aligned vectors is more extended perpendicularly to the alignment direction than is usually the case (see the compilation by Bastien & Ménard 1990). Also, there is a region to the northwest (3″ E and 36″ N) in the V and I maps with a polarization larger than at the center. LHL mentioned a similar effect, but to the southeast instead, on the opposite side of the center. To the southeast, in our maps, the polarization is lower rather than higher than the central polarization.

TABLE 5

POSITION OF THE NULL POINTS FOR V376 CAS

Bandpass	Bin (arcsec)	$\Delta\alpha$ (arcsec)	$\Delta\delta$ (arcsec)	ΔR (arcsec)	ΔZ (arcsec)
I	4	6.1	39.7	4.8	0.8
		3.1	32.0	−3.2	0.8
	1	6.8	38.3	3.8	−1.1
		4.0	32.2	−2.7	1.0
V.....	4	6.8	38.5	3.9	0.7
		4.0	34.0	−1.9	1.1
	1.5	6.0	32.0	3.8	−0.6
		7.8	37.8	−2.4	−2.7

Far from the central source, there is a centrosymmetric pattern with some deviations. A better description might be elliptical. This is seen best in the western lobe, at positions around 3″ W and 32″ N with respect to V633 Cas, where the polarization P.A. is $\approx$0° over a large area. This effect is more pronounced in the I and 9000 Å maps.

3.2.2. *V633 Cas*

Figure 3 shows the polarization maps for V633 Cas, in V and I. In the literature, maps are available in V and I and at 9000 Å. At long wavelengths, a centrosymmetric pattern typical of reflection nebulae is seen over most of them. This is in agreement with the maps presented by Piirola et al. (1992) also in I, and by LHL at 9000 Å. However, the radius of curvature of the centrosymmetric pattern becomes longer at shorter wavelengths. A possible explanation for this effect is that at shorter wavelengths the source appears bigger because of the larger optical depth.

Slightly remote from V633 Cas, a zone in which the polarization goes to zero is detected easily in our I map and in LHL's 9000 Å map. It is located $\sim$5″ north of the star. This feature is not present in the V map. It suggests the presence of an embedded source that begins to dominate the polarization at that position at long wavelengths but does not contribute at shorter wavelengths. This is discussed further in § 4.2 below.

The complication introduced by the proximity of (at least) two sources, V633 Cas and V633 Cas B, makes it impossible to compare the polarization map with calculations of a double scattering model (Bastien & Ménard 1990), and also Monte Carlo calculations (e.g., Ménard 1989; Ménard & Bastien 1996) that include only one light source.

3.3. *Direct Imaging*

A comparison with the field star PSF shows that extended nebulosity is associated with both program stars (Fig. 1). This circumstellar material extends quite far, 20″ and 45″ respectively for V376 (Figs. 4, 5 [Plates 7–8], and 6) and V633 Cas (Figs. 7, 8 [Plates 9–10], and 9). An infrared K-band image of V376 Cas is presented in Figure 10.

On each one of the $BVRI$ images, we compared the relative positions of V633 and V376 Cas with the positions of the five brightest field stars common to all frames. To evaluate the errors, we compared the positions of 21 detectable stars on four successive frames taken in I. The maximum spread in position was 0.13 pixel, $\sim$0.″06 (1 σ), yielding 3 σ uncertainties of $\sim$0.″2. The results are presented in Table 6 and Figure 11. The uncertainties on the positions given in Figure 11 depend on the number of individual images in each bandpass. The reference position is from the I frame. In Table 6, the columns give (1) the name of the star, (2) the bandpass, the apparent displacement of the photocenter in (3) right ascension, $\Delta\alpha$, and (4) in declination, $\Delta\delta$, from the I-band reference position, (5) the mean uncertainty of the position of the star in both coordinates, $\sigma_{\alpha,\delta}$, and (6) the mean uncertainty for these displacements, σ_d.

From Figure 11*a*, the position of V376 Cas changes with wavelength, while this is not the case within the uncertainties for V633 Cas (Fig. 11*b*). For V376 Cas, it is important to note that the displacement is measured on frames in

FIG. 4*b*

ASSELIN et al. (see 472, 353)

PLATE 8

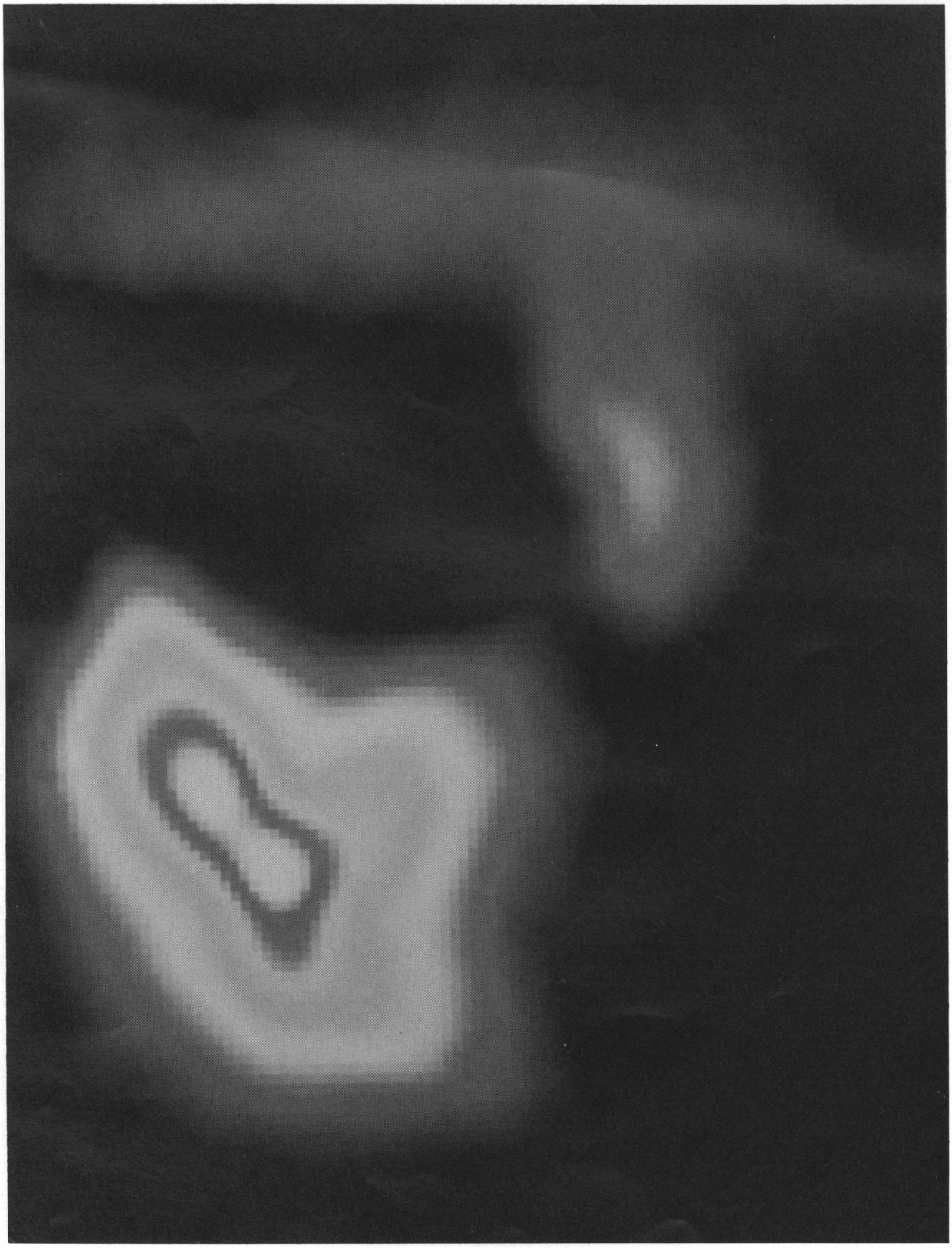

FIG. 5*b*

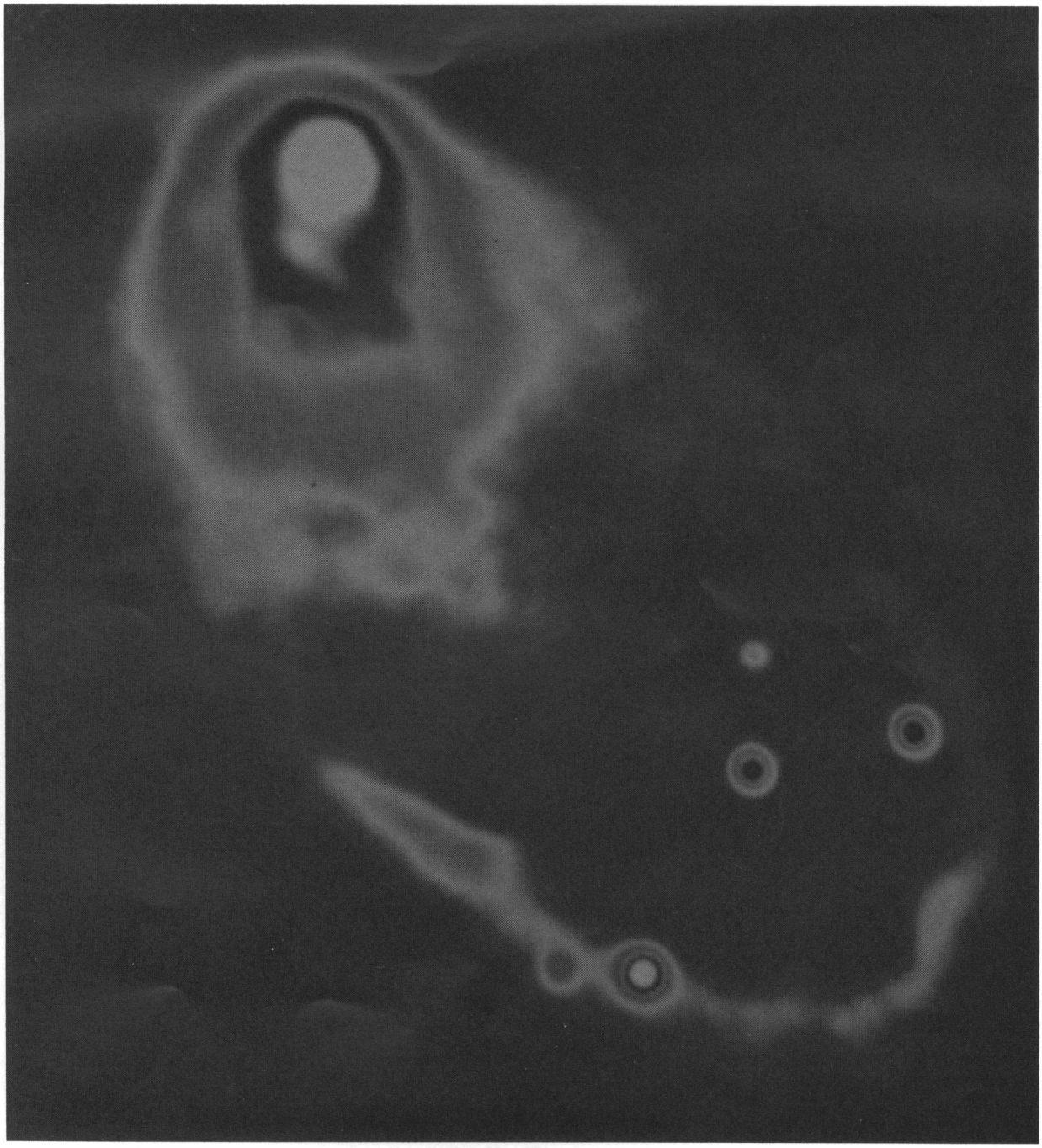

FIG. 7*b*

ASSELIN et al. (see 472, 353)

PLATE 10

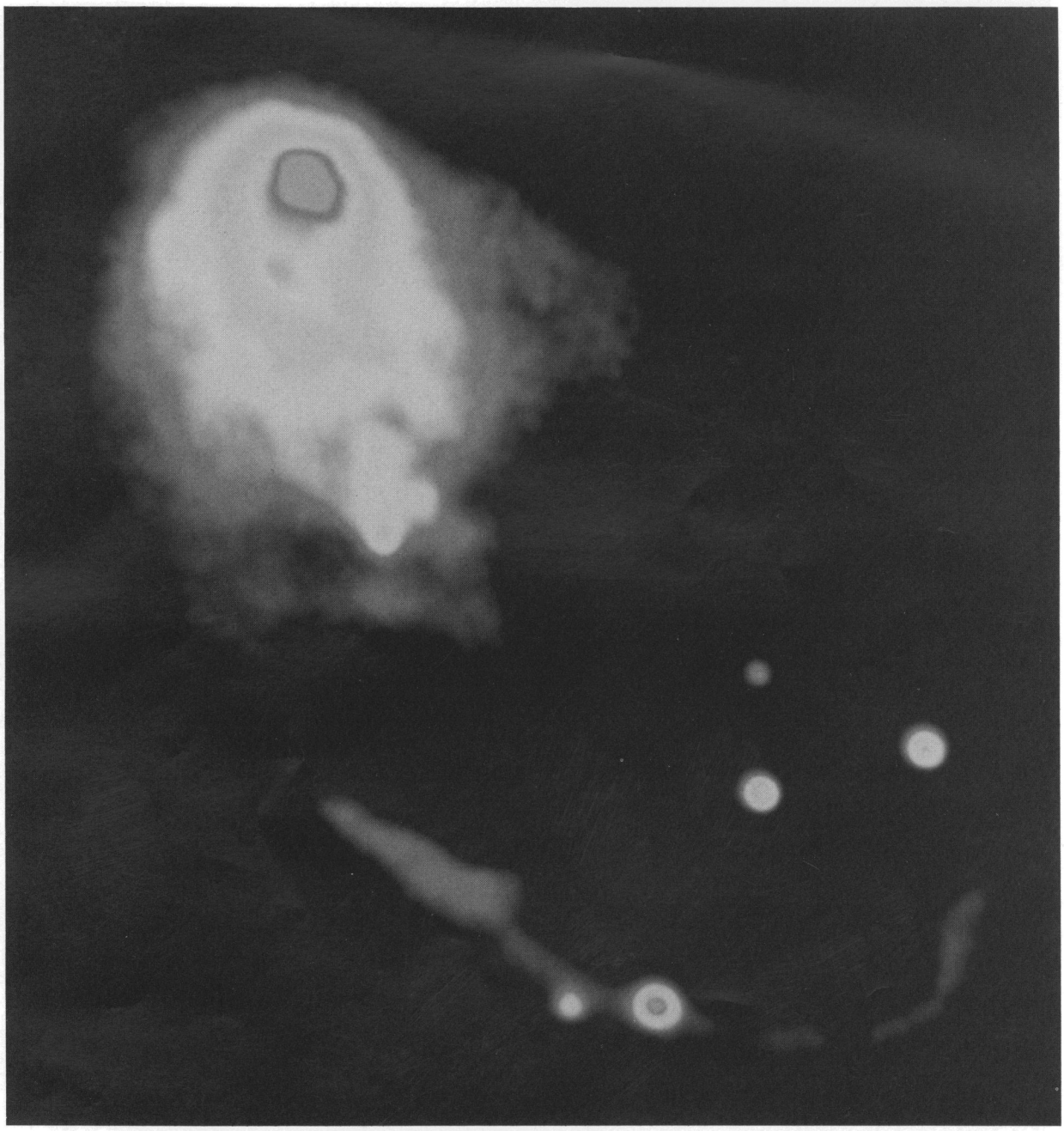

FIG. 8*b*

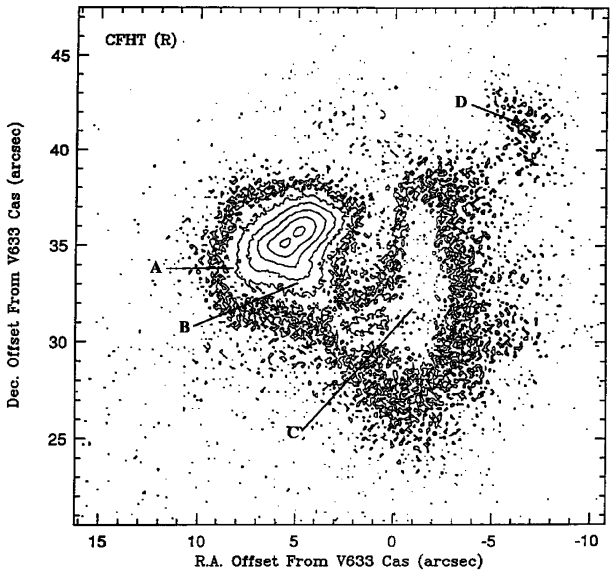

FIG. 4*a*

FIG. 4.—*R*-image of V376 Cas taken at CFHT. (*a*) Direct image with contours scaled logarithmically from the peak down to 2 σ above sky level. The position of the various features (labeled A–D) described in the text is also shown. (*b*) A maximum entropy deconvolution of (*a*).

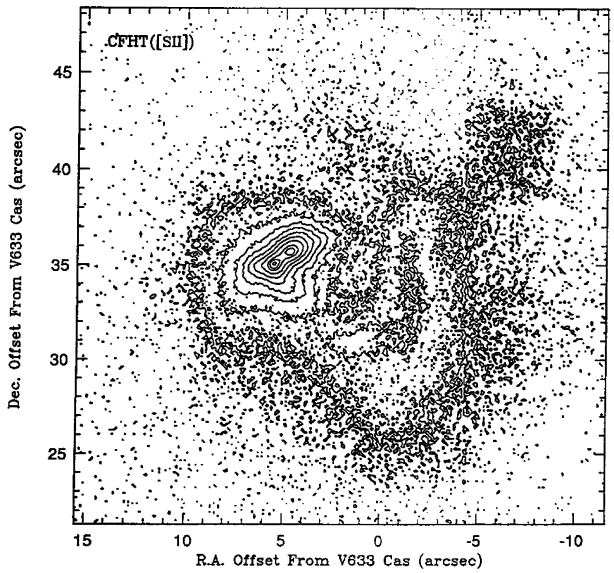

FIG. 5*a*

FIG. 5.—V376 Cas in a narrow-band [S II] filter obtained at the CFHT. (*a*) Contour plot of the direct image. The contours are scaled down logarithmically from the peak to 2 σ. (*b*) A maximum entropy deconvolution of the same image, shown in gray scale.

which the double peaks (see § 3.3.1 below) are not resolved. The displacement of the apparent image position is along position angle 240° and reaches up to ~0".7 west and ~0".3 south in *B* relative to the *I* position. This displacement is much smaller than the one measured for L1551 IRS 5 in a narrower wavelength range, namely, ~1".35 between the Gunn *i* and *r* filters (Campbell et al. 1988).

Such a displacement of the apparent position of the photocenter with wavelength has been measured only for a few stars so far: GL 490 (Campbell, Persson, & McGregor 1986), L151 IRS 5 (Campbell et al. 1988), NGC 7538 (Campbell & Persson 1988), L1489 (Emerson & Moore 1995), and HL Tau (by examining carefully the images of Weintraub et al. 1992). To explain these displacements, Ménard (1993) invoked the presence of an optically thick disk seen close to edge-on. Because the optical thickness changes with wavelength, radiative transfer calculations showed that the effective trajectories of photons received by an observer are deviated by various amounts from a straight line. At short wavelengths, the photons escape more easily in a direction perpendicular to the disk before being scattered toward the observer. This results in the apparent position of the star being displaced toward the edge of the disk. At long wavelengths the disk is more transparent and the stellar image appears closer to its actual position in space.

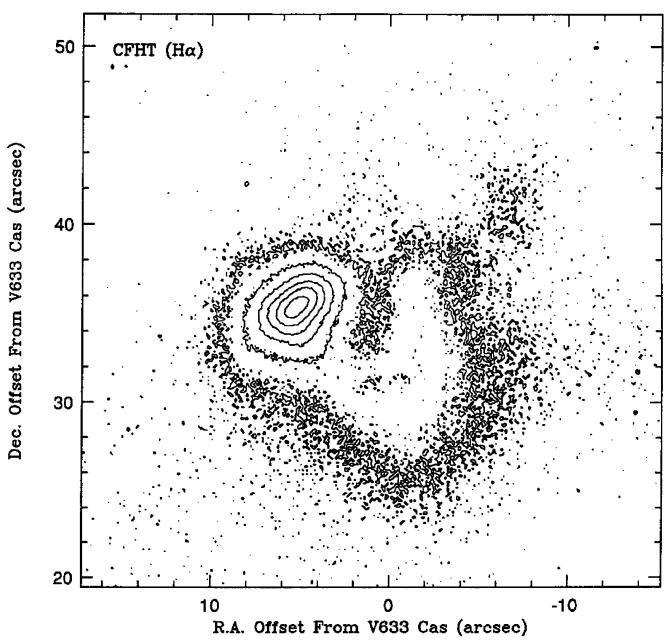

FIG. 6.—Contour plot of V376 Cas in Hα, obtained at CFHT. Contours are scaled down logarithmically from the peak to 2 σ.

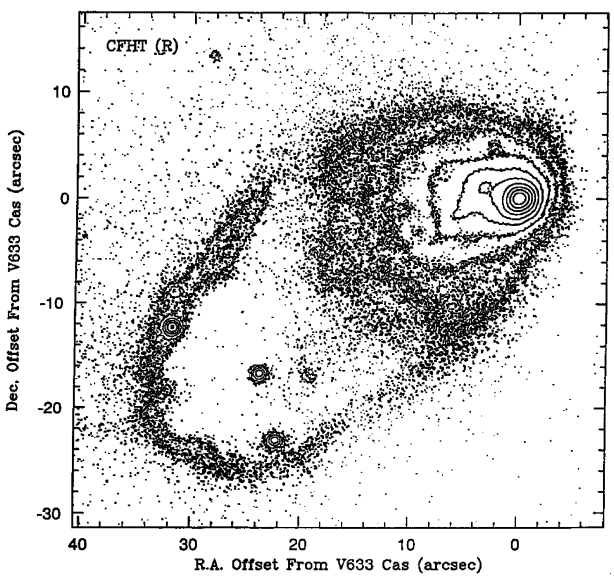

FIG. 7*a*

FIG. 7.—V633 Cas in an *R* image from the CFHT. (*a*) Direct image with contours scaled down logarithmically from the peak to 2 σ above local sky level. (*b*) A maximum entropy deconvolution of (*a*) in a gray-scale format.

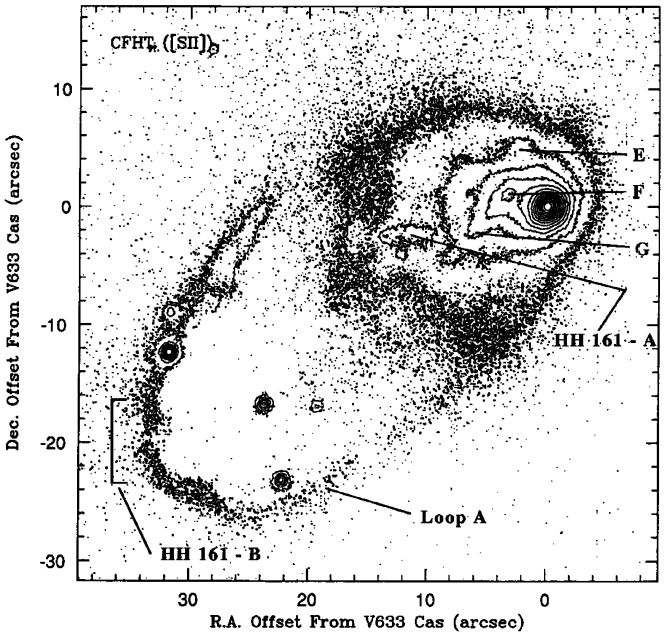

FIG. 8a

FIG. 8.—V633 Cas in an [S II] image from the CFHT. (*a*) Contour plot of the direct image with contour scaled logarithmically from the peak down to 2 σ above the local sky level. The position of the various features described in the text (labeled E–G, HH 161 A) is also indicated. (*b*) A maximum-entropy deconvolution of the same image in a gray-scale format.

3.3.1. *The Circumstellar Environment of V376 Cas*

On Figure 4*a* are identified the various features observable in the V376 Cas nebulosity that will be discussed in § 4. They are labeled A–D.

Contour plots of *R* and [S II] images taken at the CFHT in 1989 with very good seeing conditions and higher spatial resolution are presented for V376 Cas in Figures 4*a* and 5*a*, respectively. They reveal the presence of two peaks at the centre of the images. These peaks are reported here for the first time. They are $\approx 1\farcs05$ apart at a position angle of $\approx 130°$, and they have a similar brightness, to within a few percent. Figures 4*b* and 5*b* are maximum entropy deconvolutions of Figures 4*a* and 5*a*, respectively, and are shown in gray scale.

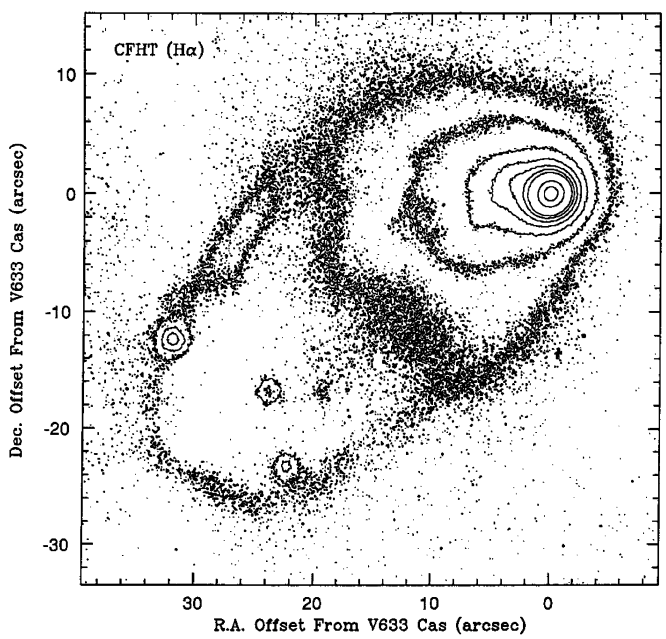

FIG. 9.—Contour plot of V633 Cas in Hα, image from CFHT data. Contours are scaled down logarithmically from the peak to 2 σ above local sky level.

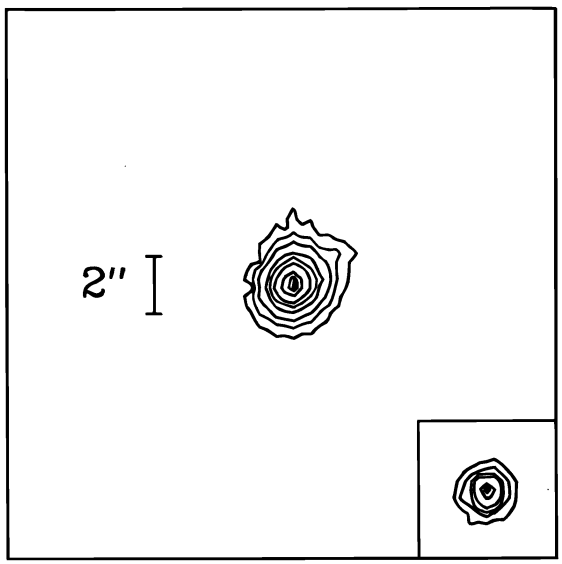

FIG. 10.—*K* image of V376 Cas. The contours are 5 and 10 σ, then 2, 5, 10, 20, 50, 80, and 95% of peak. The dynamical range of the image is ≈ 1000. North is up, and east is to the left. The lower right box displays the reference star at the same angular scale (contours at 2, 5, 10, 20, 50, 80, and 95% of peak), showing the PSF used for the deconvolution.

These peaks are not seen in the lower resolution images taken in *UBVRI* at OMM or in Hα at the CFHT in 1989 and 1993 (Fig. 6; see Table 1 for seeing conditions). The two peaks have not been detected by LHL and Piirola et al. (1992) either. Nevertheless, all these images suggest an elongation of the central source in approximately the same direction as the line joining the two [S II] peaks reported here.

The 1993 CFHT data were obtained with HR Cam to check for the two peaks in Hα with better resolution than natural seeing, HR Cam providing tip-tilt correction. Figure 12 shows the intensity profile, averaged over five columns, and parallel to the elongation of V376 Cas (at a P.A. of $\approx 135°$). We fitted the profile by three Gaussians, one for each of the two emission peaks and a broader one to

TABLE 6

OFFSETS OF THE PHOTOCENTERS FROM THE *I*-BAND POSITION

Object (1)	Bandpass (2)	$\Delta\alpha$ (arcsec) (3)	$\Delta\delta$ (arcsec) (4)	$\sigma_{\alpha,\delta}$ (arcsec) (5)	σ_d (arcsec) (6)
V633 Cas.....	*B*	0.150	0.047	0.08	0.09
	V	0.129	0.014	0.08	0.09
	R	0.052	0.020	0.06	0.08
	I	0.000	0.000	0.05	...
V376 Cas.....	*B*	−0.672	−0.306	0.08	0.09
	V	−0.505	−0.203	0.08	0.09
	R	−0.262	−0.116	0.06	0.08
	I	0.000	0.000	0.05	...

NOTE.—$\sigma_{\alpha,\delta}$ is the mean uncertainty of the position of the star in both coordinates; σ_d is the mean uncertainty of the distance of the star from the *I* band in both coordinates.

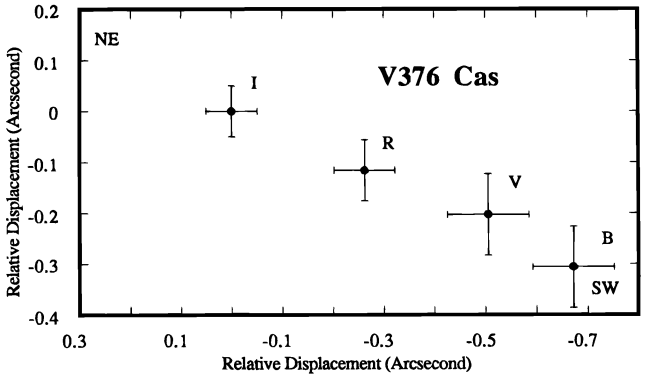

FIG. 11*a*

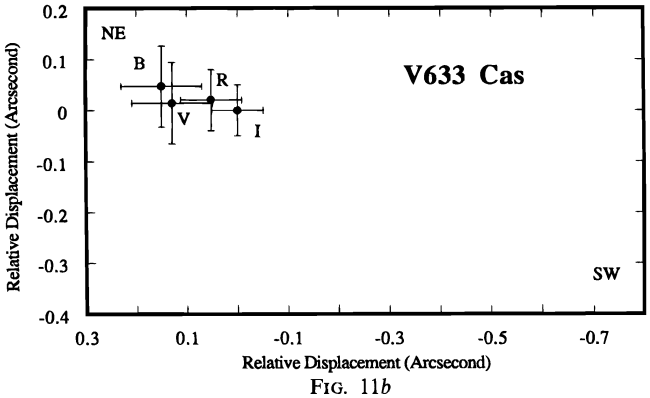

FIG. 11*b*

FIG. 11.—Position of the optical centroids as a function of wavelength for (*a*) V376 Cas, and (*b*) V633 Cas. The *I* position is used as a reference. The error bars show the uncertainty of the mean position in a given filter and are functions of the number of frames collected.

represent the extended emission in the vicinity. In the fit we forced the separation of the two narrow Gaussians to be exactly that measured between the [S II] peaks. On Figure 12, the northwest shoulder visible in the data is well fitted, suggesting that the corresponding emission peaks in Hα and [S II] have a similar origin. On the 6840 Å image of LHL, it is the northwest peak that is brighter, suggesting strong variability. Unfortunately, the date of their observation is not given. The implications of this result will be discussed in § 4.1.

Features A and B are protuberances, deviations from elliptical contours in the isophotes close to the central source(s). Feature A extends parallel to the line joining the two emission peaks, while B extends perpendicularly to it and appears connected to the southeastern component. There is also a feature (C) extending to the west and southwest of the central objects, and another one to the northwest (D). C and D are probably traces of a large reflection nebula. Feature D shows up better on the contours of the deconvolved image (not shown here)

The *K*-band image (Fig. 10) has been taken under subarcsecond seeing conditions. The FWHM of the PSF is 0.″6, measured on the reference star and confirmed by the central core of the V376 Cas profile. On Figure 10, V376 Cas seems asymmetrical, with an elongation in the northwest direction at P.A. ≈ 335°. At the resolution of our observations, there is no sign that V376 Cas is a binary star. Deconvolutions of V376 Cas by the reference star using three different algorithms (CLEAN, Lucy, and a maximum entropy–based method in the IRAF package) all resulted in V376 Cas being pointlike with emission extending ∼3″ at P.A. ≈335°,

3.3.2. *The Circumstellar Environment of V633 Cas*

The large-scale "bubble" that can be seen extending over 45″ SE of V633 Cas is visible in both the emission lines (Fig. 8) and the continuum (Fig. 1). Following CRB, we call it "loop A." Fits of ellipses to it give a position angle of 128° ± 3° (see Asselin 1991 for the details). Most of it is in fact scattered light, as it is not visible on the [S II]–r_n difference image of CRB (their Fig. 1*d*), except for a small portion to the southeast that they labeled "knot B," and which is part of HH 161. Another, much fainter, loop is also visible on deep images (e.g., CRB), "Loop B." These loops are

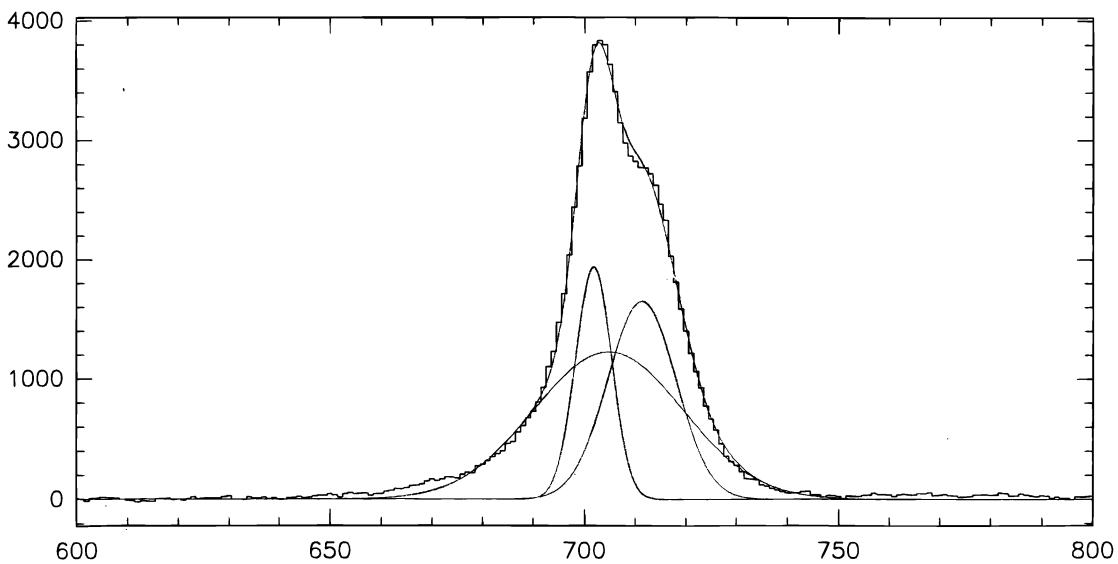

FIG. 12.—Cut in the Hα image obtained in 1993 December over five columns at a P.A. of ≈135° (northwest is to the right). The data (histogram) has been fitted by three Gaussians, two for the emission peaks and a broader one for the extended emission. The sum of the three Gaussians is shown by a thin line fitting the data.

presumably the optical counterparts of the red wing CO outflow (Levreault 1988; Nakano et al. 1990). Also, three emission knots, one of them right on V633 Cas, have been identified by CRB as a jet emanating from V633 Cas at $\approx 160°$. There is another emission knot on the opposite side, to the northwest, which might correspond to a counterjet. These four knots constitute HH 164.

The other features surrounding V633 Cas are identified in Figure 8*a*. They are labeled E, F, G, and HH 161 A. Feature E lies to the northeast of V633 Cas. Its position coincides closely with the position of the null point seen in the polarization map in the *I* band (see § 3.2.1). It is also very close to the infrared source, V633 Cas B, reported by Lagage et al. (1993) and CRB.

Feature F corresponds to a small intensity peak located almost on the axis of loop A. It is aligned with other protuberances in the intensity contours (G), with a P.A. of $\approx 136°$, in reasonable agreement with the large-scale direction. It is not detected in Hα but is clearly visible in *R*. Although the positions and morphologies of features F and G suggest a jet on the axis of the large bubble, these features do not show on the difference image [S II]–r_n of CRB.

HH 161 A is a jetlike condensation observed in [S II] only; it is the same as "knot A" discussed by CRB. Together with "knot B" of CRB, it makes HH 161. The position angle of HH 161 A is $\sim 100°$ with respect to V633 Cas, but is not very well in line with it. [S II] emission knots are the most prominent indicators of outflows, and this knot was already reported as being blueshifted by Strom et al. (1986).

The three bright sources located at the southeast end of loop A are detected in all the wide-band Johnson filters. This rules out a possible Herbig-Haro nature for them, the latter being detected normally in emission lines only (Mostly [S II] and Hα). They are probably field stars.

It is clear now that the environment of V633 Cas is complex, made of numerous features and multiple sources. A comprehensive model is difficult to construct, but some ideas will be discussed in § 4.2 below.

4. DISCUSSION

4.1. *Is V376 Cas a Double or a Single Star?*

The general aspect of the nebulosity surrounding V376 Cas is quite complex, and although it does not look similar to the typical bipolar reflection nebula, it shows some clear characteristics of it. Its very large linear polarization is an example. It is generally understood in terms of a star surrounded by a reflection nebula that scatters and polarizes light but whose direct (unpolarized) photons are blocked somehow and cannot reach the observer. The easiest way to block these photons in large enough quantities without also having an extinction in excess of what is observed is to invoke the presence of an equatorial disk (optically thick but geometrically thin) seen edge-on (e.g., Ménard & Bastien 1992). Numerical simulations showed that large values of linear polarization can be obtained in such geometries if the optical thickness is large enough. A natural consequence of that is the occurence of multiple scattering (Bastien & Ménard 1988). The detection of circular polarization in V376 Cas supports this explanation (Gravel & Bastien 1996). We notice that the small displacement of the image centroids measured as a function of wavelength occurs at $\approx 70°$ to the direction of elongation of the source.

However, the main difference between this object and other YSOs is the fact that *two* peaks are detected in the intensity maps (Figs. 4 and 5), as discussed in § 3.3.1. Their nature is intriguing, and three interpretations seem possible: a guiding error during observations, a double star with an $\approx 1''$ separation, and a single star with an edge-on disk.

A guiding error on our images is ruled out because only V376 Cas appears double, while V633 Cas and all other field stars do not, all having a one-peak PSF. One could also advocate the straightforward explanation that V376 Cas is a binary star. The fact that images with similarly good resolution obtained at CFHT in Hα (in 1993) and by Piirola et al. (1992) in *I* show only elongated contours instead of two peaks can be explained by time variability of the two "light sources." We showed in § 3.2.1 that a good fit to these elongated profiles is obtained with a geometry similar to the one needed to explain the two [S II] emission peaks. However, our *K*-band image (Fig. 10) does not show V376 Cas as a double star, even after deconvolution. Since the optical depth is smaller in the near-IR than in the optical, we would have expected the two stars of a binary system to be detected more easily in *K*, the more so since the FWHM of the image is about half the separation between the suspected stars. This is not the case; V376 Cas appears single, and it is a strong argument against V376 Cas being an $\approx 1''$ binary system surrounded by a common envelope.

Also, a large polarization of V376 Cas, almost perpendicular to the projected axis of the hypothesized binary, cannot be explained easily by the binary model. As shown by calculations (Berger & Ménard 1996), if V376 Cas were a binary system embedded in a common envelope of ellipsoidal shape, a linear polarization of 23% would require an extremely opaque scattering envelope ($\tau_{ext} \sim 15$–25). The two stars would again be much more difficult to detect in the optical than in the infrared, in contradiction with the *K* image presented in Figure 10.

On the other hand, if we are looking at a single star with an equatorial disk seen edge-on, the observed polarization pattern is well explained. It is a typical aligned vector pattern surrounded by a centrosymetric field, as expected in bipolar reflection nebulae (Bastien & Ménard 1988). Also, because the direct unpolarized starlight is absorbed by the disk, the fraction of scattered light is large, and the integrated polarization ($\sim 23\%$) can be explained. Furthermore, our images of V376 Cas show the correct behavior with wavelength if the system is a bipolar reflection nebula: the total size of the nebula decreases as λ increases, and the contours are more elongated at shorter wavelengths, becoming pointlike at longer ones. Remarkable images showing this behavior have been presented by Rouan et al. (1988), for example, for IRAS 09371+1212. The images by LHL and Piirola et al. (1992) show the same behavior, with the same orientation. The speckle interferometry by LHL shows that the orientation of this structure holds at all spatial scales, including their unresolved central region at < 100 AU.

A tentative explanation for the peaks we detect is the fact that they may trace enhanced [S II] line emission at these positions. Since [S II] is included in the R filter, they may also be detected in that filter, given they are bright enough. Their absence in other filters (especially in Hα) might be either because that line is not emitted remotely from the star

(hence not spatially resolved) or because of time variability, since the best seeing images available are not simultaneous. There is evidence for such strong variability in the literature (see § 3.2.1).

At a distance of 600 pc, the separation of the two knots means that the [S II] line is emitted at 300 AU above and below the disk plane, in a zone that corresponds to the base of the lobes in a bipolar reflection nebula. This interpretation supports the model in which emission lines are produced at the base of the jet, away from the disk. The two zones are visible because the disk is very closely edge-on. Pudritz, Pelletier, & Gomez de Castro (1991) have proposed that an hydromagnetic disk wind would recollimate and produce a "magnetic focal point" at which shocks could be responsible for the forbidden line emission. Typical values of 100 AU above and below the disk plane for the position of the "focal points" are expected for T Tauri stars, and the value we measure here for a more massive star, 300 AU, is compatible with the fact that these objects may have larger flow velocities (Mundt & Ray 1994).

These two separated emission peaks could also be the result of a single extended reflection nebula whose bright central part is hidden by an edge-on disk. The resulting intensity contours would then show two bright spots separated from one another. In the near-infrared, the disk would become optically thinner, the two bright spots would move closer, and only one intensity peak would be detected, as observed.

The orientation of these two peaks is in agreement with the orientation of the bipolar nebula traced by the inner contours seen in all filters. Also, the angle between the integrated polarization (and also the aligned vector zone) is about perpendicular, to within $\approx 15°$, to the line joining the two peaks, as expected for a bipolar reflection nebula.

Both interpretations imply that at least one Herbig Ae/Be star has an equatorial disk.

4.2. *Where is the Source of the Outflow in V633 Cas?*

Strom et al. (1986) argued that there is a strong tendency for optical outflows of YSOs to be aligned along the direction of the magnetic field threading the host molecular cloud. The alignment of flows with the magnetic field may offer fundamental clues regarding the role played by the field during the early phases of stellar formation and possible wind collimation mechanisms. LHL measured the polarization in five bandpasses for 14 stars within 2° of the two program stars. They found an average P.A. of $67° \pm 14°$ for the polarization, which gives also the direction of the magnetic field. This is quite different from the direction of the optical and radio outflows for V633 Cas. Therefore, it seems that the magnetic field apparently did not play a dominant role in the early evolution of this star. This is in agreement with the results of Goodman et al. (1990), stating that the magnetic field may not be the dominant factor for cloud evolution on scales smaller than 1 pc.

From our polarization maps, we see that there is a polarization null point at the position of feature E in I but not in V. This suggests that an embedded source is hidden at that position, or close to it. This is very close to the position of the infrared source V633 Cas B discovered recently 6″ north of V633 Cas. V633 Cas B is much closer to the major axis of the flow traced by loop A and suggests that V633 Cas B is driving the outflow, not V633 Cas itself. This was suggested first by Asselin (1991) and Lagage et al. (1993). However, CRB showed that the blueshifted emission HH 161 A and another knot in loop A are associated with V633 Cas B. Also, V633 Cas has a jet at P.A. = 160° that apparently excludes this star as being the origin of both HH 161 and loop A. Therefore, V633 Cas B, if it is the source of both HH 161 and loop A, cannot also be the source of the redshifted molecular outflow, unless it is itself a binary and each component has its own outflow. More likely is the possibliity that another source in the region, the submillimeter source $\approx 21''$ NW of V633 Cas found by Hajjar & Bastien (1994, 1996), drives the molecular outflow. In fact, this source lies at the center of two HCO + elongated structures (Nakano et al. 1990), oriented almost perpendicularly to the outflow direction (Hajjar & Bastien 1996). These structures could be the signature of a molecular disk around the new source.

The fact that there are at least two outflows and that at least two confirmed sources exist in that complex makes it a rather complicated system, comparable to the HL/XZ Tau complex. It also means, unfortunately, that previous near-IR photometry probably included both sources and that models based on only one source to explain the spectral energy distribution of V633 Cas may have to be revised to include V633 Cas B. This IR companion will probably result in a lowering of the parameters of the disk often invoked to produce the near- and mid-IR excess (Natta et al. 1992), especially its size and accretion rate as well as the importance of the envelope.

4.3. *Implications for the Binary Formation Mechanism*

Here we adopt the scenario that V376 Cas is a single star with an edge-on disk ($i = 90°$). Nearby, there are at least two other objects (see Fig. 1), V633 Cas and V633 Cas B. V633 Cas is at a projected distance of 37″ (or 22,000 AU) south from V376 Cas, and V633 Cas B is about 6″ north (or 3600 AU) of V633 Cas. The outflow direction for these sources are 130° for V376 Cas (P.A. of the two peaks), 128° (loop A), or 135° (HH 161 A; CRB) for V633 Cas B, and 160° (HH 164; CRB) for V633 Cas. The fact that V633 Cas and V633 Cas B seem to be the driving sources of outflows that have different orientations suggests that their respective disks (supposed perpendicular to the flow) are not coplanar. The other sources in the field do not seem associated with this region of the molecular cloud L1265.

If all three stars originated from the same molecular cloud or cloud fragment, then a plausible initial configuration is that of an elongated cloud (see, e.g., Bonnell & Bastien 1993). Based on the results of these simulations and on the fact that the disks are not coplanar, the axis of rotation of the original cloud had to be at an arbitrary angle with respect to the cloud axis. On the other hand, if the original cloud had an oblate rather than prolate configuration, with the short axis oriented in the east-west direction, then it seems improbable that it could have produced these three stars with noncoplanar disks. Given the large projected separations, we cannot rule out the possibility that tidal effects may have reoriented the disks. These arguments also hold if V633 Cas and V633 Cas B form a binary system with V376 Cas not being physically associated with them.

5. SUMMARY

We studied the pre–main-sequence stars V376 Cas and V633 Cas with optical direct and polarimetric imaging, optical aperture polarimetry and infrared imaging.

The main result of this work is that there is strong evidence that V376 Cas is associated with an equatorial disk. The arguments in support of this are as follows:

1. The very large (and time-variable) linear polarization observations are best explained by the presence of an equatorial disk seen very close to edge-on, a point supported further by the shape of the polarization pattern close to the central source. V376 Cas is the most highly polarized pre–main-sequence star measured so far.

2. In [S II] and *R*, the intensity maps show two peaks $\approx 1\farcs05$ apart at P.A. = 130°. These peaks are detected at other wavelengths (especially in Hα) in the form of extended, elongated emission shoulders. These profiles are again well explained by an edge-on disk. Either the intensity peaks are two zones of enhanced emission (at least in [S II]) located at the base of a jet on both sides of the disk, or they are the inner part of a bright reflection nebula whose center is obscured by the disk. The brightness of these peaks seem to vary with time. These observations may have implications for the line emission mechanism. Spectroscopy of the two knots would help to decide.

The region surrounding V633 Cas (LkHα 198) is very complex and final conclusions are difficult to draw:

1. There are at least two sources: V633 Cas and an IR source located $\approx 6''$ north of it, V633 Cas B. There is also a submillimeter source $\approx 21''$ NW of V633 Cas. The fact that two sources, close to one another, contribute to the measured spectral energy distribution implies that models including only one source have to be revised.

2. V633 Cas probably drives a jet at P.A. = 160°, HH 164. On the other hand, V633 Cas B is probably responsible for the jet associated with HH 161. It lies also on the axis of the large loop seen in the optical at P.A. ≈ 128° and is therefore the most likely candidate for being its source. These HH objects and molecular flows suggest that equatorial disks are present around the stars.

3. The aperture linear polarization of V633 Cas is suspected to be variable.

The conclusions drawn here about the presence of circumstellar disks around Herbig Ae/Be stars admittedly rest on observations of two objects only (or three, with V633 Cas B), objects that may very well be peculiar amongst this class of pre–main-sequence stars. Nevertheless, and although models without disks exist to explain the properties of these stars, it seems that observations of at least some members of this class require an equatorial disk.

Grateful thanks are given to Jacques Richer and Pierre Gravel for their help for the deconvolution of the CFHT images. We would like to thank the directors of the Canada-France-Hawaii Telescope and Observatoire du Mont Mégantic for generous telescope time allotments. Sincere thanks to go the staff and telescope operators at both observatories for their constant and precious help with the observations. F. M. thanks the Fonds pour la Formation de Chercheurs et L'Aide à la Recherche (FCAR) for a post-doctoral fellowship. This work was supported by the Natural Sciences and Engineering Research Council (NSERC) of Canada and the Québec Government.

REFERENCES

Angel, J. R. P., & Landstreet, J. D. 1970, ApJ, 160, L147
Asselin, L. 1991, M. Sc. thesis, Univ. Montréal
Bastien, P. 1982, A&AS, 48, 153; 513
———. 1987, ApJ, 317, 231
Bastien, P., & Ménard, F. 1988, ApJ, 326, 334
———. 1990, ApJ, 364, 232
Bastien, P., Ménard, F., Asselin, L., & Turbide, L. 1989, in Proc. 4th IAP Astrophysics Meeting on Modelling the Stellar Environment, ed. P. Delache, S. Lalöe, C. Magnan, & J. Tran Thanh Van (Gif-sur-Yvette: Editions Frontières), 185
Berger, J. P., & Ménard, F. 1996, in preparation
Böhm, T. 1993, Ph.D. thesis, Univ. Paris VII
Bonnell, I., & Bastien, P. 1993, ApJ, 406, 614
Campbell, B., & Persson, S. E. 1988, AJ, 95, 1185
Campbell, B., Persson, S. E., & McGregor, P. J. 1986, ApJ, 305, 336
Campbell, B., Persson, S. E., Strom, S. E., & Grasdalen, G. L. 1988, AJ, 95, 1173
Corcoran, D., Ray, T. P., & Bastien, P. 1995, A&A, 293, 550 (CRB)
Catala, C. 1989, in ESO Proc. No. 33, Low Mass Star Formation and Pre–Main-Sequence Evolution, ed. B. Reipurth (Garching: ESO), 471
Emerson, J. P., & Moore, T. J. T. 1995, in Polarization of the Interstellar Medium, ed. W. Roberge & D. C. B. Wittet (San Francisco: ASP), in press
Goodman, A. A., Bastien, P., Mayers, P. C., & Ménard, F. 1990, ApJ, 359, 363
Gravel, P., & Bastien, P. 1996, in preparation
Hajjar, R., & Bastien, P. 1994, JRASC, 88, 262
———. 1996, in preparation
Herbig, G. H. 1990, ApJS, 4, 337
Hillenbrand, L. A., Strom, S. E., Vrba, F. J., & Keene, J. 1992, ApJ. 397, 613
Lada, C. J., & Adams, F. C. 1992, ApJ, 393, 278
Lagage, P. O., Olofsson, G., Cabrit, S., Cesarsky, C. J., Nordh, L., & Rodriguez Espinosa, J. M. 1993, ApJ, 417, L79
Leinert, C., Haas, M., & Lenzen, R. 1991, A&A, 246, 180 (LHL)
Levreault, R. M. 1988, ApJS, 67, 283
Ménard, F. 1989, Ph.D. thesis, Univ. Montréal
———. 1993, in Proc. Graduate Workshop on Star Formation, ed. J. P. Arcoragi, P. Bastien, & R. Pudritz (Montréal: Dépt. de Physique), 161
Ménard, F., & Bastien, P. 1992, AJ, 103, 564
———. 1996, in preparation
Mundt, R., & Ray, T. 1994, in Proc. First Conference on The Nature and Evolutionary Status of Herbig Ae/Be Stars, ed. P. S. Thé, M. R. Pérez, & E. P. J. van den Heuvel (San Francisco: ASP), 237
Nakano, M., Kogure, T., Yoshida, S., & Tatematsu, K. 1990, PASJ, 42, 567
Natta, A., Palla, F., Butner, H. M., Evans, N. J. II, & Harvey, P. M. 1992, ApJ, 391, 805
———. 1993, ApJ, 406, 674
Piirola, V., Scaltriti, F., & Coyne, G. V. 1992, Nature, 359, 399
Pudritz, R. E., Pellitier, G., & Gomez de Castro, A. I. 1991, in the Physics of Star Formation and Early Stellar Evolution, ed. C. J. Lada, & N. D. Kylafis (Dordrecht: Kluwer), 539
Rouan, D., Lacombe, F., & Tiphène, D. 1990, CFHT Bull., 22, 1
Rouan, D., Omont, A., Lacombe, F., & Forveille, T. 1988, A&A, 189, L3
Scarrott, S. M., Draper, P. W., & Warren-Smith, R. F. 1989, MNRAS, 237, 621
Strom, K. M., Strom, S. E., Wolff, S. C., Morgan, J., & Wenz, M. 1986, ApJS, 62, 39
Weintraub, D. A., Kastner, J. H., Zuckerman, B., & Gatley, I. 1992, ApJ, 391, 784